



Low toxicity of metal-organic framework MOF-199 to bacteria *Escherichia coli* and *Staphylococcus aureus*

Bowei Ouyang^a, Peng Ouyang^a, Mengyao Shi^a, Tusunniyaze Maimaiti^a, Qun Li^a, Suke Lan^a, Jin Luo^{c,*}, Xian Wu^{a,b}, Sheng-Tao Yang^{a,b,*}

^a Key Laboratory of Pollution Control Chemistry and Environmental Functional Materials for Qinghai-Tibet Plateau of the National Ethnic Affairs Commission, School of Chemistry and Environment, Southwest Minzu University, Chengdu 610041, China

^b Key Laboratory of General Chemistry of the National Ethnic Affairs Commission, School of Chemistry and Environment, Southwest Minzu University, Chengdu 610041, China

^c Analytical and Metrical Center of Sichuan Province, Chengdu 610023, China



ARTICLE INFO

Keywords:

Metal-organic framework
Bacteria
Toxicity
DNA damage
Oxidative stress
Environmental safety

ABSTRACT

Metal-organic framework (MOF) materials are emerging materials for various applications because of their unique structures and properties. The hazards and environmental safety of MOF should be carefully evaluated before their large-scale production. Herein, we studied the toxicity and its mechanisms of MOF-199 to Gram-negative bacterium (*Escherichia coli*) and Gram-positive bacterium (*Staphylococcus aureus*). MOF-199 was synthesized from Cu(NO₃)₂ and 1,3,5-benzenetricarboxylic acid by hydrothermal method and well characterized before toxicological evaluations. MOF-199 was nontoxic to bacteria at low concentrations, and the bacterium growths were completely inhibited at high concentrations (900 mg/L for *E. coli*; 1200 mg/L for *S. aureus*). Cell deaths occurred at high MOF-199 concentrations associated with the loss of cytoplasm and flagella. The toxicological mechanisms of MOF-199 were attributed to oxidative stress, which further led to the membrane damage and DNA damage. The chemical origin of MOF-199 toxicity should be partially attributed to the released Cu²⁺ in culture medium, because Cu(NO₃)₂ was much more toxic than 1,3,5-benzenetricarboxylic acid. Our results indicated that MOF-199 was of low toxicity and environmental risks to bacteria.

1. Introduction

Metal-organic framework (MOF) materials are the rising star materials in recent years, which are formed by the chelation between metal ions and organic ligands (Furukawa et al., 2013). More than 67,000 papers on MOF were found in Science Citation Index (SCI) database. MOF materials have many advantages, such as easy preparation protocols, low producing costs, large surface areas and pore volumes, and good stability (Sharma and Feng, 2017; Luo et al., 2019; Shu et al., 2020). Due to the fantastic properties, MOF materials are widely applied in diverse areas. For instance, MOF materials show great potential in gas separation and purification (Lin et al., 2017). MOF materials could be used for carbon capture and conversion (Wu et al., 2019). MOF materials are high-performance catalysts for various reactions (Xiao and Jiang, 2019). MOF materials are regarded as superior adsorbents for metal ions (Wang et al., 2020). MOF materials show great performance in energy area (Du et al., 2020), and biomedical area (Lan et al., 2017). Beyond the successful achievements, the hazards and toxicity of MOF materials should be systematically evaluated to ensure their safe applications (Sajid, 2016).

The toxicity and safety of MOF materials have aroused the concerns of the community, but the toxicological data of MOF materials are still seldom reported in literature. MOF materials showed low toxicity to mammalian cells (Yen et al., 2016; Chen et al., 2019; Lin et al., 2016; Hu et al., 2014). For instance, Wagner et al. measured the IC₅₀ (50 % inhibiting concentration) for MIL-160 and ZIF-8 in human bronchial epithelial cells (421 and 57 µg/mL) and human non-small cancer lung cells (433 and 61 µg/mL) (Wagner et al., 2019). Both cells showed decreased resistance and alpha parameter only at high MOF concentrations. IRMOF-3 led to cell death, viability loss, membrane damage at 100 and 400 µg/mL (Ren et al., 2014). Similarly, the *in vivo* studies suggested that MOF accumulated in body and induced low toxicity to animals (Destefani et al., 2016). Simon-Yarza et al. reported that MIL-100 was fast cleared from blood with high hepatic accumulation (45 %) with meaningful liver toxicity (Simon-Yarza et al., 2016). Nontoxic Fe (III)-MOF accumulated in reticuloendothelial system after intravenous injection and aroused significant oxidative stress (Baati et al., 2013). Beyond that, Fan et al. reported the environmental hazards of MOF to *Microcystic aeruginosa* (Fan et al., 2018). Cu-MOF-74 inhibited the *M. aeruginosa* growth at 1 mg/L and higher. Therefore, MOF materials have

* Corresponding authors.

E-mail addresses: luojin sns@163.com (J. Luo), yangst@pku.edu.cn (S.-T. Yang).

potential toxicity and risks after entering the environment. The toxicological mechanism and chemical origin of MOF toxicity are still largely unknown and require further investigations.

MOF-199 (also known as HKUST-1) is a representative MOF material for catalysis (Sun et al., 2015), adsorption (Ma et al., 2018), separation (Tadjarodi and Abbaszadeh, 2016), chemical sensing (Hosseini et al., 2016), drug delivery (Decoste et al., 2012), and luminescence sensor (Homayoonnia and Zeinali, 2016). In this study, we performed a systematic toxicological study of MOF-199 on Gram-negative bacterium (*Escherichia coli*) and Gram-positive bacterium (*Staphylococcus aureus*), which were widely used in environmental toxicity evaluations (Zhang et al., 2020; Wu et al., 2018). MOF-199 was synthesized by hydrothermal method and characterized by scanning electron microscopy (SEM), X-ray photoelectron spectroscopy (XPS), X-ray diffraction (XRD), infrared spectroscopy (IR) and Raman spectroscopy. The toxicity of MOF-199 was studied by growth curve, colony-forming unit (CFU) count, cell death rate and ultrastructure. The toxicological mechanism was explored by measuring the membrane damage indicator, comet assay and parameters of oxidative stress. The release of Cu²⁺ and the toxicity of starting materials were also evaluated to identify the chemical origin of MOF-199 toxicity. The implications to the environmental hazard assessments and safe applications of MOF materials are discussed.

2. Materials and methods

2.1. Preparation of MOF-199

MOF-199 was synthesized by hydrothermal method following the literature protocol and characterized by multiple techniques (Hamon et al., 2010). Cu(NO₃)₂•3H₂O (1.05 g) was dissolved in a

30 mL of 50/50 (v/v) water-ethanol mixture. After adding 1,3,5-benzenetricarboxylic (0.5 g), the solution was added into a Teflon liner and the liner was further sealed in an autoclave for hydrothermal reaction at 393 K for 24 h. After cooling, the product was sonicated for 5 min in aforementioned water-ethanol mixture. The turquoise-blue solids were isolated by filtration and dried in air for 1 d. The obtained MOF-199 was characterized by XRD (XD-6, Purkinje General Instrument Co., China), XPS (ESCALAB 250XI, Thermo-Fisher, USA), IR (Magna-IR 750, Nicolet, USA), SEM (JSM-7500, JEOL, Japan) and Raman spectroscopy (inVia, Renishaw Co., UK).

2.2. Exposure of bacteria to MOF-199

E. coli and *S. aureus* were purchased from Guangdong Culture Collection Center and cultured following the recommended protocols. Lysogeny broth (LB) medium was consisted of peptone (10 g/L), NaCl (10 g/L) and yeast extract (5 g/L) for *E. coli* culture. Trypticase (tryptic) soy broth (TSB) medium was consisted of pancreatic digest of casein (17 g/L), enzymatic digest of soybean meal (3 g/L), NaCl (5 g/L), dextrose•H₂O (2.5 g/L) and KH₂PO₄ (2.5 g/L) for *S. aureus* culture. The pH was adjusted to 7.2 for both media before use. The bacterium strain was inoculated in liquid culture medium and cultured in a shaker for 12 h. The medium was diluted to the final density of 6000 cells/mL for inoculation in the toxicological evaluations. For bacterium exposure, MOF-199 was dispersed into culture medium at 0–1200 mg/L and sterilized. The inoculation densities were set as 6 × 10³ cells/mL (*E. coli*) and 2 × 10⁶ cells /mL (*S. aureus*) in 50 mL liquid culture medium. After the incubation at 37 °C for 0–36 h, the bacteria were collected for toxicological evaluations.

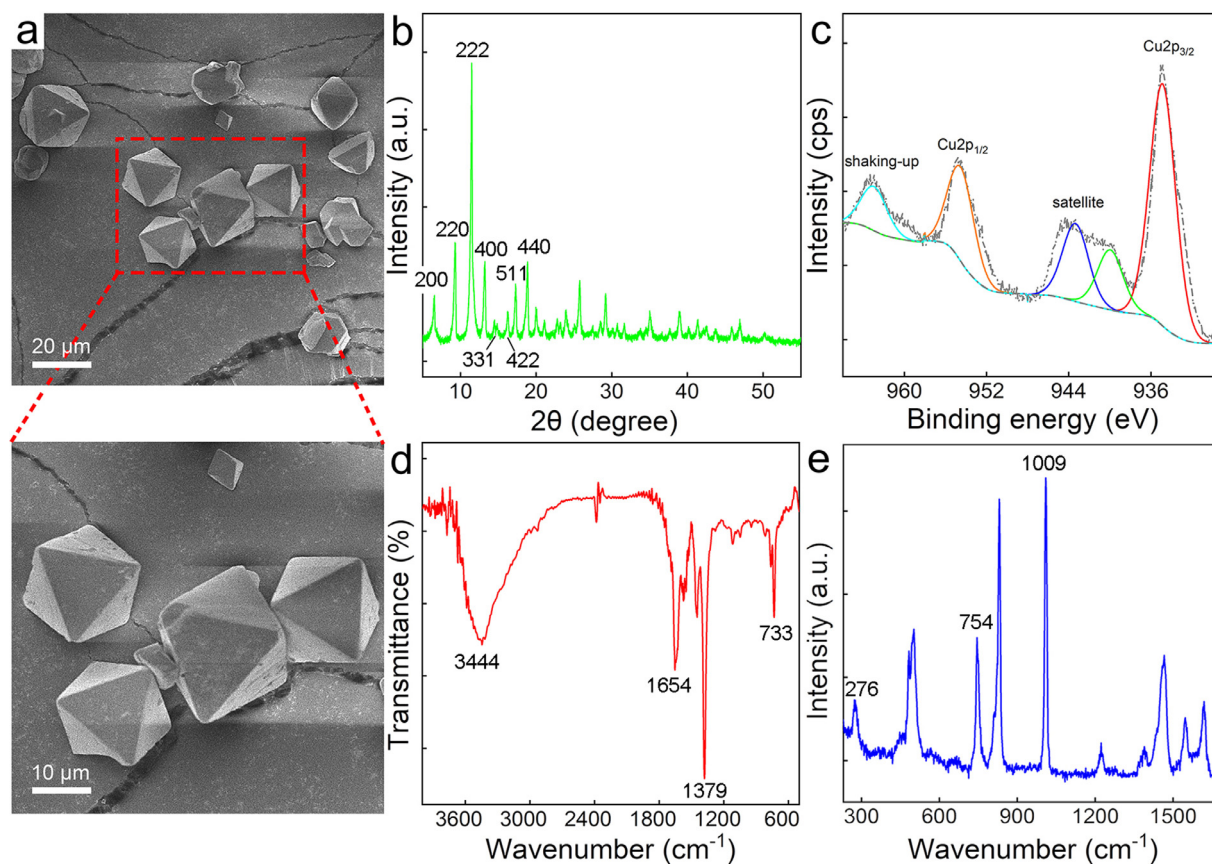


Fig. 1. Characterization data of MOF-199 sample. (a) SEM images. The red box was SEM image of higher magnification; (b) XRD spectrum; (c) Cu2p XPS spectrum; (d) IR spectrum; (e) Raman spectrum.

2.3. Bacterial growth

For growth curve, the optical density at 600 nm (OD_{600}) was recorded with 3 h interval for each flask. It should be noted that the blue MOF-199 was not dispersible in culture medium, thus the blue color of MOF-199 did not affect the OD_{600} measurements. For CFU counts, 50 μ L of bacterium suspension was taken at 9 and 36 h after the exposure. After serial dilution, the bacterium suspension was inoculated on solid medium and the colony number was counted with a colony counter at 48 h (Scan-300, Wisdom Shanghai Instrument Co., China).

2.4. Bacterial survival rate

The bacterium suspensions (500 μ L for each) were taken at 9 and 36 h, centrifuged (4500 rpm \times 10 min) to remove the supernatant, and re-suspended in 200 μ L of 0.85 % NaCl. To the cell suspension, 2 μ L mixture of DMAO stock solution and ethidium homodimer-III (EthD-III) stock solution (v:v of 1:2) was added to each sample. After thorough mixing with a vortex mixer, the mixture was incubated for 15 min in dark at room temperature. The fluorescence images were recorded on a fluorescence microscope (Axio Vert. A1, Zeiss, Germany) for survival rate counting. All bacteria were stained in green by DMAO and only the dead ones were stained in red by EthD-III.

2.5. Membrane damage, oxidative stress and DNA damage

The bacterial cells were collected at 9 and 36 h by centrifugation. The cells were homogenized for 500 s (60 Hz) to prepare cell suspensions for oxidative stress. The levels of total protein, lactate dehydrogenase (LDH), peroxidase (SOD), glutathione (GSH) and malondialdehyde (MDA) were analyzed following the manufacturer's instructions (Nanjing Jiancheng Bioengineering Institute, Nanjing, China). The bacterial cells collected at 9 and 36 h by centrifugation were re-suspended in 100 μ L phosphate buffer saline for each sample. The DNA damage was measured by comet assay following the literature protocol (COMPAC-50, Cleaver Scientific, UK) (Solanky and Haydel, 2012).

2.6. Cu^{2+} release in culture medium

MOF-199 was shaken in liquid culture medium at 120 rpm and 37 °C. At designed time points, the medium was centrifuged (10000 rpm \times 10 min) to remove MOF-199 residues. For Cu concentration determination, the samples were diluted with 2 % HNO_3 for inductively coupled plasma-mass spectrometry (ICP-MS, iCAP-Qc, Thermo-Fisher, USA) measurements.

2.7. Statistical analysis

All data were analyzed as the mean with the standard deviation (mean \pm SD). Significance was calculated by Student's *t*-test, and $p < 0.05$,

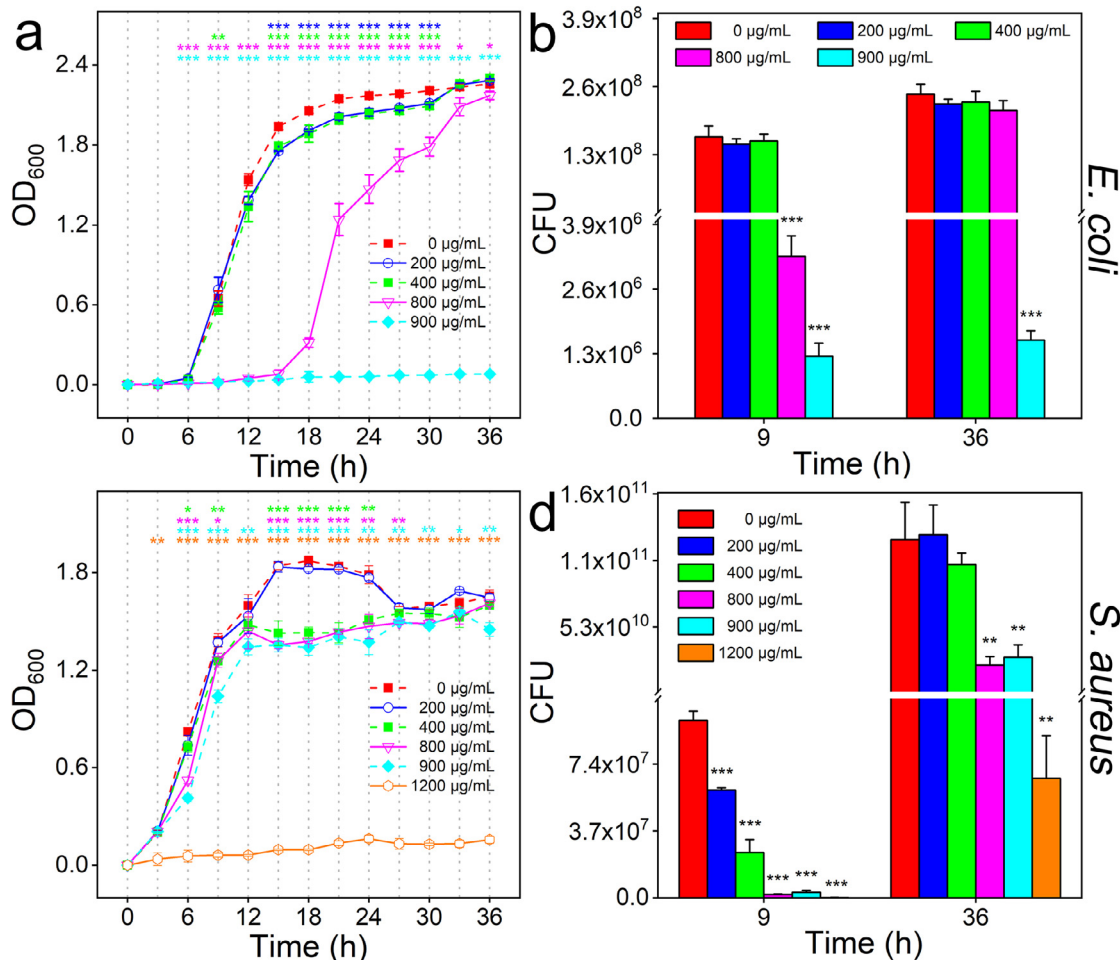


Fig. 2. Influence of MOF-199 on the bacterial growth ($n = 3$). (a) Growth curve of *E. coli*; (b) CFU of *E. coli*; (c) Growth curve of *S. aureus*; (d) CFU of *S. aureus*. * $p < 0.05$, ** $p < 0.01$, and *** $p < 0.001$ compared with the control group.

$p < 0.01$ and $p < 0.001$ were taken as the standards of statistical significance (Guan et al., 2020).

3. Results and discussion

3.1. Characterization of MOF-199

MOF-199 were micro-particles with double-pyramid structure under SEM (Fig. 1a). Some double-pyramids stacked over to form irregular structures. The diameters of MOF-199 ranged from 5–20 μm . The non-uniform appearance of MOF-199 under SEM was consistent with the literature observations (Hamon et al., 2010). The typical XRD spectrum of MOF-199 was obtained, well consistent with the literature results (Hamon et al., 2010). As reported by Chui et al., MOF-199 was a cubic network, where Cu₂-clusters were coordinated by the carboxylate groups to give paddle-wheel unit and these primary building blocks were connected through the H₃BTC ligand into a three-dimensional cubic network (Chui et al., 1999). In Cu2p XPS spectrum, the sig-

nals of Cu indicated the presence of Cu²⁺ in MOF-199, corresponding to the Cu₂-clusters. The IR spectrum of MOF-199 indicated the presence of -OH at 3444 cm^{-1} . The observation of 1654 cm^{-1} peak and the lack of 1710 cm^{-1} peak indicated the deprotonation of -COOH groups in 1,3,5-benzenetricarboxylic acid after chelating with Cu²⁺ (Nguyen et al., 2012). The symmetric stretch of the unbound 1,3,5-benzenetricarboxylic acid ligand was slightly shifted to lower frequency (1379 cm^{-1}) upon coordination to Cu²⁺. The Cu-O bond was evidenced by the peak at 733 cm^{-1} . MOF-199 showed meaningful Raman peaks at 276, 483, 501, 745, 830, 1009, 1223, 1465, 1546 and 1619 cm^{-1} , consistent with the previous report (Lange and Obendorf, 2015). The peak at 276 cm^{-1} was attributed to the stretching vibration mode of Cu-Cu bonding. The peak at 745 cm^{-1} corresponds to C-H stretching. The peak at 1009 cm^{-1} was due to the aromatic C-C bond antisymmetric stretching. All aforementioned characterization data collectively indicated that MOF-199 was successfully synthesized for toxicological evaluations (Hamon et al., 2010; Solanky and Haydel, 2012; Schlichte et al., 2004; Nguyen et al., 2012; Lange and Obendorf, 2015).

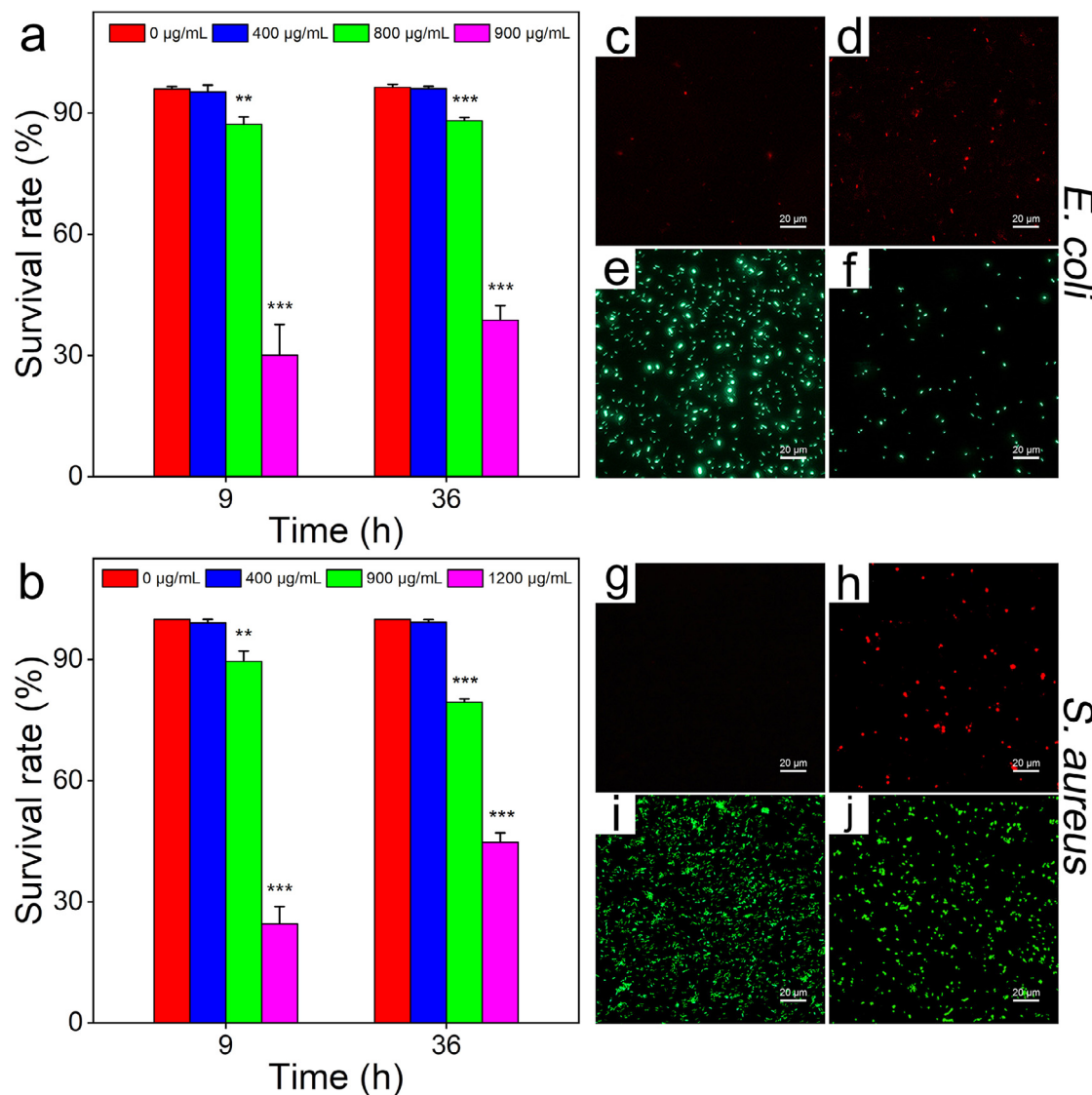


Fig. 3. Bacterial survival rates upon the exposure to MOF-199 ($n = 3$). (a) Survival rate of *E. coli*; (b) Survival rate of *S. aureus*; (c) EthD-III staining of *E. coli* without exposure; (d) EthD-III staining of *E. coli* at 900 $\mu\text{g}/\text{mL}$ of MOF-199; (e) DMAO staining of *E. coli* without exposure; (f) DMAO staining of *E. coli* at 900 $\mu\text{g}/\text{mL}$ of MOF-199; (g) EthD-III staining of *S. aureus* without exposure; (h) EthD-III staining of *S. aureus* at 900 $\mu\text{g}/\text{mL}$ of MOF-199; (i) DMAO staining of *S. aureus* without exposure; (j) DMAO staining of *S. aureus* at 900 $\mu\text{g}/\text{mL}$ of MOF-199. * $p < 0.05$, ** $p < 0.01$, and *** $p < 0.001$ compared with the control group.

3.2. Toxicity of MOF-199 to bacteria

Since the toxicity data of MOF was scarce, a large concentration range from 1-1200 $\mu\text{g}/\text{mL}$ was preliminarily evaluated before the toxicological assays. MOF-199 of lower concentrations (1-100 $\mu\text{g}/\text{mL}$) had no antibacterial effect at all (Fig. S1). Therefore, we used higher concentrations during our experiments to provide the toxic threshold and explore the hazards of MOF-199 under extreme conditions. Similarly, the literature studies also used high concentrations. For example, in Ren et al.'s study of IRMOF-3, the concentration range was 0-400 mg/L (Ren et al., 2014). The toxicity of MOF-199 was first monitored by measuring the OD₆₀₀ during the incubation (Fig. 2). For *E. coli*, the control showed typical growth curve reaching plateau after 15 h. The growth of *E. coli* was slightly inhibited at 200 and 400 $\mu\text{g}/\text{mL}$ of MOF-199. Interestingly, the growth of *E. coli* was delayed by 800 $\mu\text{g}/\text{mL}$ of MOF-199. In the first 15 h, no obvious bacterial growth was evidenced, while the OD caught up after 36 h incubation. This suggested that MOF-199 was toxic to *E. coli* but did not lead to the complete death at 800 $\mu\text{g}/\text{mL}$. Further increase of MOF-199 concentration to 900 $\mu\text{g}/\text{mL}$ led to the thorough inhibition of bacterial growth. Consistent with the growth curves, the CFU of control group and groups of low MOF-199 concentrations were

very similar for *E. coli*. The CFU of 800 $\mu\text{g}/\text{mL}$ group (2.0 % of control) was much lower than that of control at 9 h, but the values became similar at 36 h (87.2 % of control). For 900 $\mu\text{g}/\text{mL}$ group, the CFU was very small at both 9 (0.8 % of control) and 36 h (0.6 % of control). For *S. aureus*, the control group and 200 $\mu\text{g}/\text{mL}$ group showed typical growth curve reaching plateau after 12 h. The growth of *S. aureus* was slightly inhibited at 400 and 800 $\mu\text{g}/\text{mL}$ of MOF-199. The growth of *S. aureus* was completely inhibited at 1200 $\mu\text{g}/\text{mL}$. The CFU of *S. aureus* showed MOF-199 concentration dependent decreases at 9 h. The CFU of *S. aureus* recovered at 200 and 400 $\mu\text{g}/\text{mL}$. The CFU at 800 and 900 $\mu\text{g}/\text{mL}$ increased to about 20 % of control, while the CFU at 1200 $\mu\text{g}/\text{mL}$ did not recover at all. The difference between growth curves and CFU changes of *S. aureus* should be attributed to the death of bacterial cells in the logarithmic growth phase, where the dead cells were detected by OD measurements but not CFU counting. In addition, the starting material Cu(NO₃)₂ was more toxic than MOF-199 according to the growth curves and CFU, while 1,3,5-benzenetricarboxylic acid was of very low toxicity (Fig. S2&S3).

The growth inhibition by MOF-199 was observed in their applications of antibacterial materials. For example, Rodriguez et al. and Rickhoff et al. independently observed the growth inhibition of *E.*

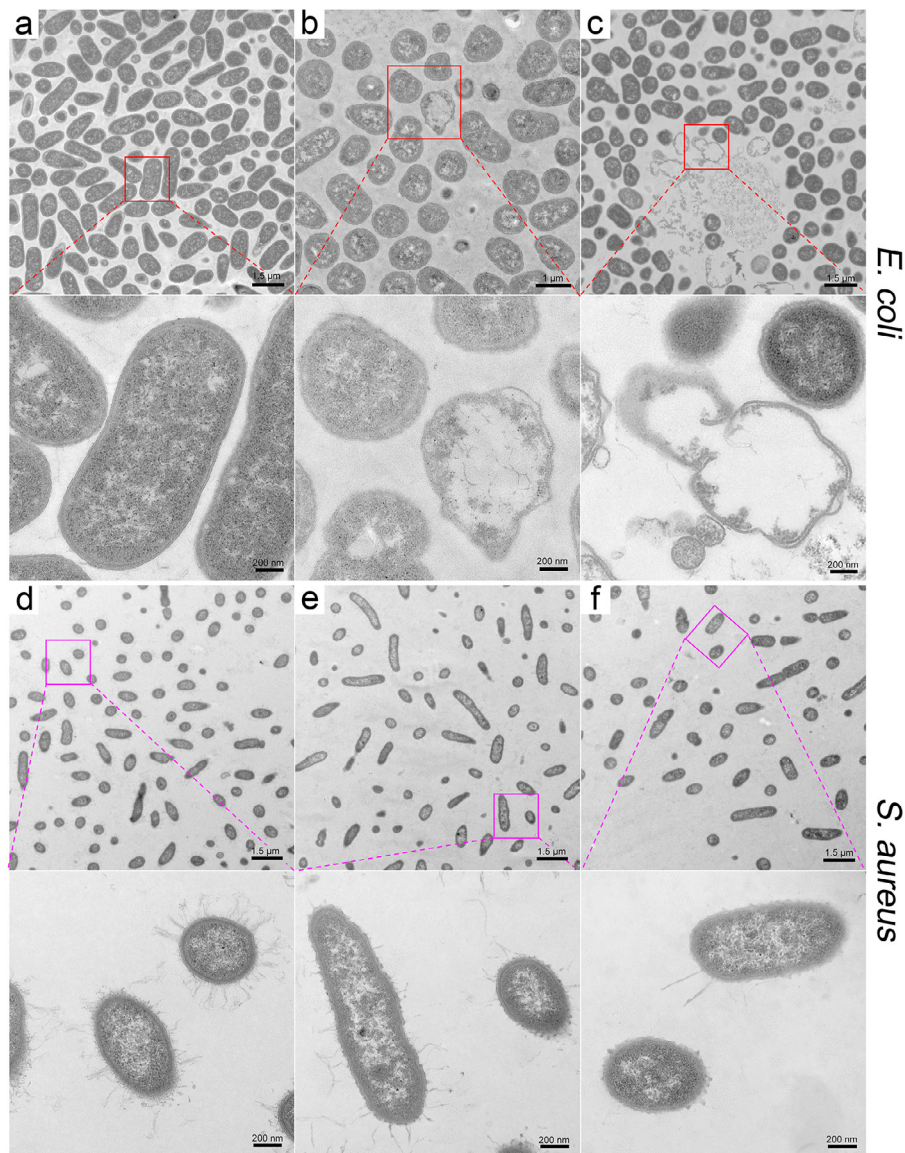


Fig. 4. Ultrastructural changes of bacteria. (a) The control of *E. coli*; (b) *E. coli* exposed to 800 $\mu\text{g}/\text{mL}$ of MOF-199; (c) *E. coli* exposed to 900 $\mu\text{g}/\text{mL}$ of MOF-199; (d) The control of *S. aureus*; (e) *S. aureus* exposed to 900 $\mu\text{g}/\text{mL}$; (f) *S. aureus* exposed to 1200 $\mu\text{g}/\text{mL}$.

coli by cellulose-MOF-199 composite material (Rodriguez et al., 2014; Rickhoff et al., 2019). It should be noted that Wang et al. observed the toxicity of cellulose-MOF-199 composite was higher to *S. aureus* than to *E. coli* in bacteriostatic zone measurements (Wang et al., 2015). The difference between Wang et al.'s results and our results might likely be due to the incorporation of cellulose, which enhanced the toxicity of MOF-199. Ren et al. found that chitosan-MOF-199 could inhibit the bacterial growth in disc diffusion assay (Ren et al., 2019). Similar applications were achieved by fabricating MOF-199 with polyester or Nylon (Enam et al., 2018). The DMSO extracted MOF-199 showed minimum inhibition concentrations of 60–70 mg/L. Ballesteros-Garrido et al. applied macroscopic chloramphenicol-MOF-199 for bacterial population control. Bulk MOF-199 could partially inhibit the growth of *E. coli*, which was further enhanced by chloramphenicol (Ballesteros-Garrido et al., 2019). However, the inhibition concentration was very high, where 1000 mg/L of MOF-199 showed inhibition effect to *E. coli*. The high inhibition concentration of MOF-199 suggested that pure MOF-199 was not ideal for antibacterial applications with low environmental toxicity.

To verify whether MOF-199 killed the bacterial cells, we stained the cells with DMAO (live and dead) and EthD-III (dead), and counted the survival rates (Fig. 3). For *E. coli*, the survival rates at 400 $\mu\text{g}/\text{mL}$ of MOF-199 were similar to the control group at both 9 and 36 h. At 800 $\mu\text{g}/\text{mL}$, the survival rates decreased to 87.2 % at 9 h and 88.1 % at 36 h. Further increase of MOF-199 concentration to 900 $\mu\text{g}/\text{mL}$ led to lower survival rates of 30.0 % at 9 h and 38.7 % at 36 h. Even after concentrating, the bacterial cells were much fewer at 900 $\mu\text{g}/\text{mL}$. The high

survival rates of *E. coli* at 800 $\mu\text{g}/\text{mL}$ suggested that the growth delay and CFU decrease were likely due to the inhibition of cell proliferation. The growth inhibition at 900 $\mu\text{g}/\text{mL}$ should be attributed to the cell death induced by MOF-199. For *S. aureus*, 400 $\mu\text{g}/\text{mL}$ of MOF-199 did not change the survival rates, either. At 900 $\mu\text{g}/\text{mL}$, the survival rates slightly decreased to 89.5 % at 9 h and 79.4 % at 36 h. At 1200 $\mu\text{g}/\text{mL}$, the survival rates decreased to 24.5 % at 9 h and recovered partially to 44.6 % at 36 h. The high survival rates of *S. aureus* at 400 and 900 $\mu\text{g}/\text{mL}$ suggested that the CFU decreases at low MOF-199 concentrations were due to the delay of bacterial growth, rather than the cell death. The growth inhibition at 1200 $\mu\text{g}/\text{mL}$ should be attributed to the cell death and proliferation inhibition. Again, Cu(NO₃)₂ induced more cell deaths than MOF-199, and 1,3,5-benzenetricarboxylic acid did not lead to cell death (Fig. S4).

The exposure to MOF-199 also changed the ultrastructure of bacterial cells (Fig. 4). Intact *E. coli* cells had rod-like shape at both ends, and their cell wall and cytoplasm seemed normal. After the incubation with MOF-199 at 800 $\mu\text{g}/\text{mL}$ for 36 h, where the cell growth caught up (Fig. 4b), *E. coli* cells were condensed into spherical shape and their cell membrane was slightly damaged. Very a few of them lost the cytoplasm. At 900 $\mu\text{g}/\text{mL}$, the ultrastructure damage became very serious. There were plenty of cells with broken cell wall and membrane, which led to the outflow of cytoplasm. Some cell fragments were presented under TEM, too. In addition, the spherical cells were smaller than those at 800 $\mu\text{g}/\text{mL}$. For *S. aureus*, there were abundant flagella surrounding the intact cell wall in the control group. At 900 $\mu\text{g}/\text{mL}$, more cells became rod-like. The cell wall was easily recognized and the cy-

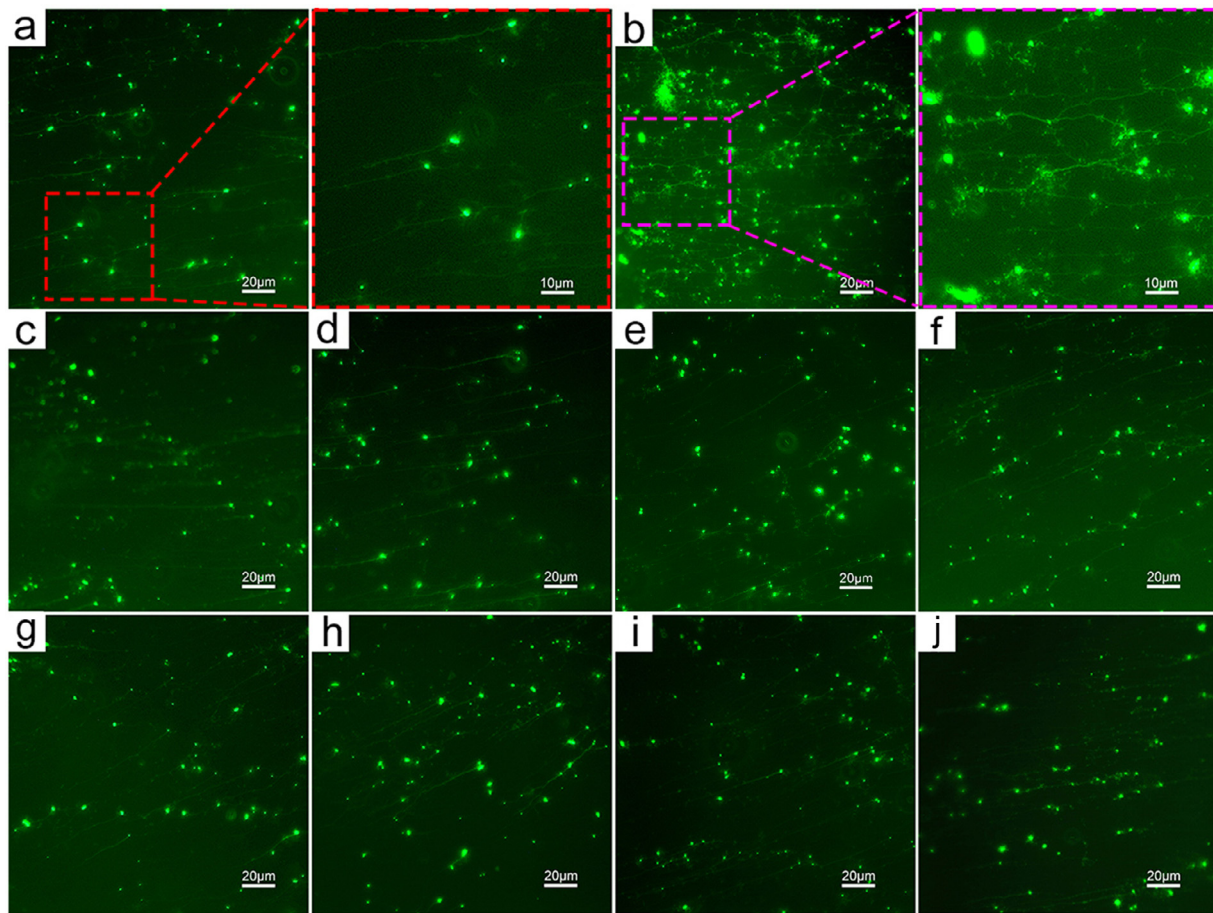
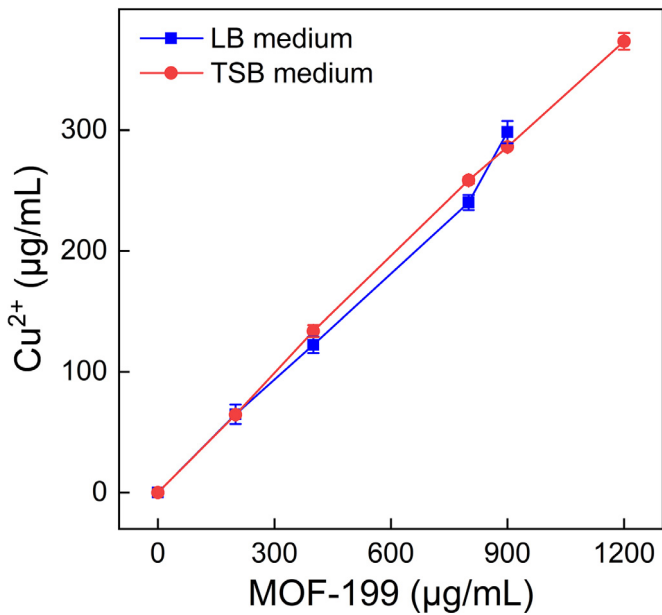
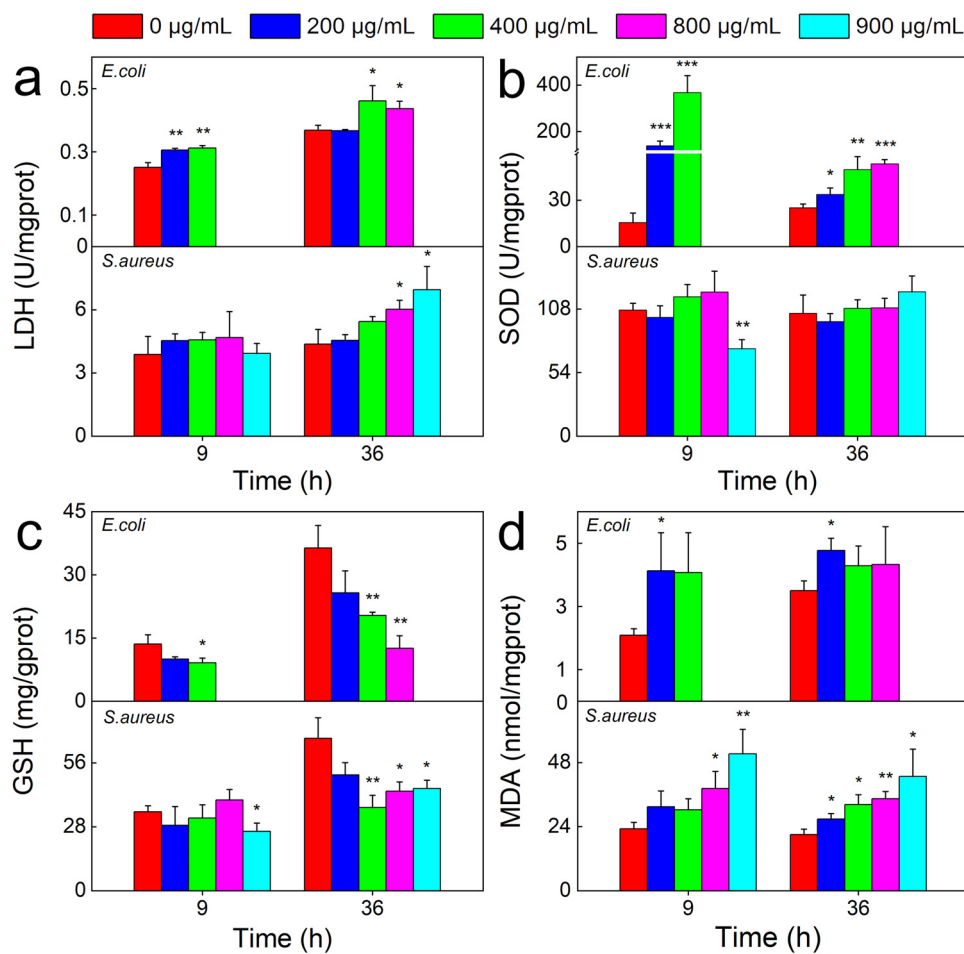


Fig. 5. DNA damage induced by MOF-199 after 36 h exposure. (a) Negative control; (b) Positive control; (c) Control of *E. coli*; (d) 400 $\mu\text{g}/\text{mL}$ (*E. coli*); (e) 800 $\mu\text{g}/\text{mL}$ (*E. coli*); (f) 900 $\mu\text{g}/\text{mL}$ (*E. coli*); (g) Control of *S. aureus*; (h) 400 $\mu\text{g}/\text{mL}$ (*S. aureus*); (i) 900 $\mu\text{g}/\text{mL}$ (*S. aureus*); (j) 1200 $\mu\text{g}/\text{mL}$ (*S. aureus*).



toplasm was kept intracellular. At the high MOF-199 concentration of 1200 $\mu\text{g/mL}$, *S. aureus* cells lost the flagella. The cell wall became invisible, suggesting the membrane damage. It should be noted that both bacteria did not swallow MOF-199, which might be due to the compact

cell wall. For those phagocytes, MIL88A could transport into Kupffer cells (Durymanov et al., 2019). MIL-100(Fe) could be faster internalized by J774 cells than HeLa cells, resulting in higher toxicity to J774 cells (Tamames-Tabar et al., 2014). This suggested that the cellular uptake of MOF should be carefully considered in their toxicological evaluations.

There was DNA damage induced by MOF-199, too (Fig. 5). In the comet assay, the control cells showed short tails and the positive cells had long tails. There were elongated tails observed in both bacteria exposed to MOF-199. Consistent with the cell growth and survival rate measurements, $\text{Cu}(\text{NO}_3)_2$ induced more membrane leakage and DNA damage than 1,3,5-benzenetricarboxylic acid (Fig. S5&S6). Separately, well consistent with the TEM observation, LDH levels increased at high concentrations after 36 h exposure to MOF-199 for both bacteria (Fig. 6a). The LDH leakage was more serious for *S. aureus*. This could be explained by the nearly total loss of cell wall of *S. aureus* in TEM observations after the exposure to MOF-199 at 1200 $\mu\text{g/mL}$. Such membrane leakage was reported in mammalian cells exposed to MIL-100(Fe) (Chen et al., 2019).

3.3. Toxicological mechanism of MOF-199 to bacteria

Oxidative damage was proposed to be the general toxicological mechanism of MOF-199 (Fig. 6). GSH levels decreased at 400 and 800 $\mu\text{g/mL}$ for *E. coli*, and the MDA levels increased at 200 $\mu\text{g/mL}$. In addition, SOD levels in *E. coli* increased at 200 $\mu\text{g/mL}$ and higher, which could be regarded as the protective response to oxidative stress. For *S. aureus*, the GSH decreases and MDA increases were observed, too. The difference was that SOD levels did not increase. These indicators suggested that MOF-199 induced oxidative damage to bacteria, which fur-

ther led to the DNA damage and membrane damage. MIL-88A and MIL-100 were also reported to arouse oxidative stress in mice (Baati et al., 2013).

As aforementioned, at nontoxic MOF-199 equivalent concentrations, Cu²⁺ already induced the growth delay and inhibition. Meaningful cell deaths, stronger membrane leakage and DNA damage were observed, too. The toxicity was so high that enough cells could not be collected for oxidative stress measurements at high Cu(NO₃)₂ concentrations (Fig. S7, S8&S9). The toxicity of Cu²⁺ to bacteria has been well documented in the literature, showing very similar phenomena to our observations (Riggle and Kumamoto, 2000). In particular, Cu²⁺ induced toxicity to bacteria through the generation of toxic reactive oxygen species in a Fenton-type reaction (Solioz et al., 2010). The observed oxidative damage (Fig. 5) in our study supported this pathway. Another possibility of Cu²⁺ toxicity was that copper specifically damaged the iron-sulfur clusters of isopropylmalate dehydratase, led to ion release to arouse oxidative stress and DNA damage (Macomber and Imlay, 2009). On the other hand, even at the highest MOF-199 equivalent concentrations that bacterial growths were completely inhibited, the chelating ligand 1,3,5-benzenetricarboxylic acid only slightly delayed but not inhibited the bacteria growth. 1,3,5-benzenetricarboxylic acid did not lead to the death of bacterial cells, either. Therefore, we speculated that the toxicity of MOF-199 originated from the Cu²⁺ release. To confirm this hypothesis, we measured the release of Cu²⁺ in culture medium (Fig. 7). MOF-199 released Cu²⁺ to culture medium efficiently in both culture media with very similar Cu contents at 36 h. In LB culture medium, the Cu²⁺ content reached 298 μg/mL at 900 μg MOF-199/mL. In TSB culture medium, the Cu²⁺ content was 373 μg/mL at 1200 μg MOF-199/mL. The release of Cu²⁺ from MOF-199 was also reported by other studies (Emam et al., 2018; Ballesteros-Garrido et al., 2019; Durymanov et al., 2019). However, the Cu²⁺ concentration here was not high enough to induce toxicity to bacteria (Fig. S3-S6), so the release of Cu²⁺ was only the partial reason of toxicity. Beyond the release of Cu²⁺, there might be other toxicological pathways, e.g. mechanical damage and toxicity directly from MOF-199 particles.

4. Conclusions

In summary, the hazards of MOF-199 to bacteria were systematically investigated, where the dissolution of Cu²⁺ was regarded as the chemical origin of MOF-199 toxicity. MOF-199 was of low toxicity to bacteria and inhibited the bacterium growth only at concentrations higher than 800 mg/L. Obvious cell deaths, the loss of cytoplasm and flagella, and meaningful DNA damage were observed. Oxidative stress was regarded as the toxicological mechanism of MOF-199. The facts that Cu²⁺ was released from MOF-199 in culture medium and Cu(NO₃)₂ was much more toxic than 1,3,5-benzenetricarboxylic acid collectively indicated that the toxicity of MOF-199 was partially from the released Cu²⁺. These results suggested that MOF-199 was of low toxicity to some specific environment. We believe that our results would benefit the environmental hazard evaluations and safe applications of MOF materials in future.

Declaration of Competing Interest

The authors declare that they have no known competing financial interests or personal relationships that could have appeared to influence the work reported in this paper.

Acknowledgments

We acknowledge financial support from the National Natural Science Foundation of China (No. 21777132), the National Program for Support of Top-notch Young Professionals, and the Fundamental Research Funds for the Central Universities, Southwest Minzu University (No. 2021PTJS36).

Supplementary materials

Supplementary material associated with this article can be found, in the online version, at doi:[10.1016/j.hazadv.2021.100002](https://doi.org/10.1016/j.hazadv.2021.100002).

References

- Baati, T., Njim, L., Neffati, F., Kerkeni, A., Bouttemi, M., Gref, R., Najjar, M.F., Zakhama, A., Couvreur, P., Serre, C., 2013. In depth analysis of the *in vivo* toxicity of nanoparticles of porous iron (III) metal-organic frameworks. *Chem. Sci.* 4, 1597–1607. doi:[10.1039/c3sc22116d](https://doi.org/10.1039/c3sc22116d).
- Ballesteros-Garrido, R., Montagud-Martinez, R., Rodrigo, G., 2019. Bacterial population control with macroscopic HKUST crystals. *ACS Appl. Mater. Interfaces* 11, 19878–19883. doi:[10.1021/acsami.9b05285](https://doi.org/10.1021/acsami.9b05285).
- Chen, G.S., Leng, X., Luo, J.Y., You, L.T., Qu, C.H., Dong, X.X., Huang, H.L., Yin, X.B., Ni, J., 2019. In vitro toxicity study of a porous iron (III) metal-organic framework. *Molecules* 24, 1211. doi:[10.3390/molecules24071211](https://doi.org/10.3390/molecules24071211).
- Chui, S.Y., Lo, M.F., Charmant, P.H., Guy Orpen, A., Williams, Lan.D., 1999. A chemically functionalizable nanoporous material [Cu₃(TMA)₂(H₂O)₃]_n. *Science* 283, 1148–1150. doi:[10.1126/science.283.5405.1148](https://doi.org/10.1126/science.283.5405.1148), -1148.
- Decoste, J.B., Peterson, G.W., Smith, M.W., Stone, C.A., Willis, C.R., 2012. Enhanced stability of Cu-BTC MOF via perfluorohexane plasma-enhanced chemical vapor deposition. *J. Am. Chem. Soc.* 134, 1486–1489. doi:[10.1021/ja211182m](https://doi.org/10.1021/ja211182m).
- Destefani, C.A., Motta, L.C., Costa, R.A., Macrino, C.J., Bassane, J.F.P., Filho, J.F.A., Silva, E.M.D., Greco, S.J., Carneiro, M.T.W.D., Endringer, D.C., 2016. Evaluation of acute toxicity of europium-organic complex applied as a luminescent marker for the visual identification of gunshot residue. *Microchem. J.* 124, 195–200. doi:[10.1016/j.microc.2015.08.021](https://doi.org/10.1016/j.microc.2015.08.021).
- Du, L., Xing, L.X., Zhang, G.X., Sun, S.H., 2020. Metal-organic framework derived carbon materials for electrocatalytic oxygen reactions: Recent progress and future perspectives. *Carbon* 156, 77–92. doi:[10.1016/j.carbon.2019.09.029](https://doi.org/10.1016/j.carbon.2019.09.029).
- Durymanov, M., Permyakova, A., Sene, S., Guo, A., Kroll, C., Gimenezmarques, M., Serre, C., Reineke, J., 2019. Cellular uptake, intracellular trafficking, and stability of biocompatible metal-organic framework (MOF) particles in Kupffer cells. *Mol. Pharmaceut.* 16, 2315–2325. doi:[10.1021/acs.molpharmaceut.8b01185](https://doi.org/10.1021/acs.molpharmaceut.8b01185).
- Emam, H.E., Darwesh, O.M., Abdelhameed, R.M., 2018. In-growth metal organic framework/synthetic hybrids as antimicrobial fabrics and its toxicity. *Colloid. Surf. B.* 165, 219–228. doi:[10.1016/j.colsurfb.2018.02.028](https://doi.org/10.1016/j.colsurfb.2018.02.028).
- Fan, G.D., Hong, L., Zheng, X.M., Zhou, J.J., Zhan, J.J., Chen, Z., Liu, S.Y., 2018. Growth inhibition of microcystic aeruginosa by metal-organic frameworks: Effect of variety, metal ion and organic ligand. *RSC Adv.* 8, 35314–35326. doi:[10.1039/c8ra05608k](https://doi.org/10.1039/c8ra05608k).
- Furukawa, H., Cordova, K.E., O'Keffe, M., Yaghi, O.M., 2013. The chemistry and applications of metal-organic frameworks. *Science* 341, 1230444. doi:[10.1126/science.1230444](https://doi.org/10.1126/science.1230444).
- Guan, X., Li, Q., Maimaiti, T., Lan, S.K., Ouyang, P., Ouyang, B.W., Wu, X., Yang, S.T., 2020. Toxicity and photosynthetic inhibition of metal-organic framework mof-199 to pea seedlings. *J. Hazard. Mater.* 409, 124521. doi:[10.1016/j.jhazmat.2020.124521](https://doi.org/10.1016/j.jhazmat.2020.124521).
- Hamon, L., Jolimaitre, E., Pirngruber, G.D., 2010. CO₂ and CH₄ separation by adsorption using Cu-BTC metal-organic framework. *Ind. Eng. Chem. Res.* 49, 7497–7503. doi:[10.1021/ie902008g](https://doi.org/10.1021/ie902008g).
- Homayonnia, S., Zeinali, S., 2016. Design and fabrication of capacitive nanosensor based on MOF nanoparticles as sensing layer for VOCs detection. *Sensor Actuat. B-Chem.* 237, 776–786. doi:[10.1016/j.snb.2016.06.152](https://doi.org/10.1016/j.snb.2016.06.152).
- Hosseini, M.S., Zeinali, S., Sheikhi, M.H., 2016. Fabrication of capacitive sensor based on Cu-BTC (MOF-199) nanoporous film for detection of ethanol and methanol vapors. *Sensor Actuat. B-Chem.* 230, 9–16. doi:[10.1016/j.snb.2016.02.008](https://doi.org/10.1016/j.snb.2016.02.008).
- Hu, Q., Yu, J.C., Liu, M., Liu, A.P., Dou, Z.S., Yang, Y., 2014. A low cytotoxic cationic metal-organic framework carrier for controllable drug release. *J. Med. Chem.* 57, 5679–5685. doi:[10.1021/jm5004107](https://doi.org/10.1021/jm5004107).
- Lan, G.G., Ni, K.Y., Lin, W.B., 2017. Nanoscale metal-organic frameworks for phototherapy of cancer. *Coord. Chem. Rev.* 379, 65–81. doi:[10.1016/j.ccr.2017.09.007](https://doi.org/10.1016/j.ccr.2017.09.007).
- Lange, L.E., Obendorf, S.K., 2015. Degradation studies of methyl parathion with CuBTC metal-organic framework. *J. Environ. Chem. Eng.* 3, 541–547. doi:[10.1016/j.jece.2015.01.007](https://doi.org/10.1016/j.jece.2015.01.007).
- Lin, R.B., Xiang, S.C., Xing, H.B., Zhou, W., Chen, B.L., 2017. Exploration of porous metal-organic frameworks for gas separation and purification. *Coord. Chem. Rev.* 378, 87–103. doi:[10.1016/j.ccr.2017.09.027](https://doi.org/10.1016/j.ccr.2017.09.027).
- Lin, W.X., Hu, Q., Yu, J.C., Jiang, K., Yang, Y.Y., Xiang, S.C., Cui, Y.J., Yang, Y., Wang, Z.Y., Qian, G.D., 2016. Low cytotoxic metal-organic frameworks as temperature-responsive drug carriers. *Chem. Plus. Chem.* 81, 804–810. doi:[10.1002/cplu.201600142](https://doi.org/10.1002/cplu.201600142).
- Luo, S.H., Zeng, Z.T., Zeng, G.M., Liu, Z.F., Xiao, R., Chen, M., Tang, L., Tang, W.W., Lai, C., Cheng, M., Shao, B.B., Liang, Q.H., Wang, H., Jiang, D.N., 2019. Metal organic frameworks as robust host of Pd nanoparticles in heterogeneous catalysis: Synthesis, application, and prospect. *ACS Appl. Mater. Interfaces* 11, 32579–32598. doi:[10.1021/acsm.9b11990](https://doi.org/10.1021/acsm.9b11990).
- Ma, S.S., Zhang, M.Y., Nie, J.Y., Yang, B., Song, S.X., Lu, P., 2018. Multifunctional cellulose-based air filters with high loadings of metal-organic frameworks prepared by growth method for gas adsorption and antibacterial applications. *Cellulose* 25, 5999–6010. doi:[10.1007/s10570-018-1982-1](https://doi.org/10.1007/s10570-018-1982-1).
- Macomber, L., Imlay, J.A., 2009. The iron-sulfur clusters of dehydratases are primary intracellular targets of copper toxicity. *Proc. Natl. Acad. Sci. USA.* 106, 8344–8349. doi:[10.1073/pnas.0812808106](https://doi.org/10.1073/pnas.0812808106).
- Nguyen, L.T.L., Nguyen, T.T., Nguyen, K.D., Phan, N.T.S., 2012. Metal-organic framework MOF-199 as an efficient heterogeneous catalyst for the aza-Michael reaction. *Appl. Catal. A-Gen.* 425, 44–52. doi:[10.1016/j.apcata.2012.02.045](https://doi.org/10.1016/j.apcata.2012.02.045).

- Ren, F., Yang, B.C., Cai, J., Jiang, Y.D., Xu, J., Wang, S., 2014. Toxic effect of zinc nanoscale metal-organic frameworks on rat pheochromocytoma (PC12) cells in vitro. *J. Hazard. Mater.* 271, 283–291. doi:[10.1016/j.jhazmat.2014.02.026](https://doi.org/10.1016/j.jhazmat.2014.02.026).
- Ren, X.Y., Yang, C.Y., Zhang, L., Li, S.H., Shi, S., Wang, R., Zhang, X., Yue, T.L., Sun, J., Wang, J.L., 2019. Copper metal-organic frameworks loaded on chitosan film for the efficient inhibition of bacteria and local infection therapy. *Nanoscale* 11, 11830–11838. doi:[10.1039/C9NR03612A](https://doi.org/10.1039/C9NR03612A).
- Rickhoff, T.A., Sullivan, E., Werth, L.K., Kissel, D.S., Keleher, J.J., 2019. A biomimetic cellulose-based composite material that incorporates the antimicrobial metal-organic framework HKUST-1. *J. Appl. Polym. Sci.* 136, 46978. doi:[10.1002/app.46978](https://doi.org/10.1002/app.46978).
- Riggle, P.J., Kumamoto, C.A., 2000. Role of a *Candida albicans* P1-Type ATPase in resistance to copper and silver ion toxicity. *J. Bacteriol.* 182, 4899–4905. doi:[10.1128/JB.182.17.4899-4905.2000](https://doi.org/10.1128/JB.182.17.4899-4905.2000).
- Rodríguez, H.S., Hinestroza, J.P., Ochoa-Puentes, C., Sierra, C.A., Soto, C.Y., 2014. Antibacterial activity against *Escherichia coli* of Cu-BTC (MOF-199) metal-organic framework immobilized onto cellulosic fibers. *J. Appl. Polym. Sci.* 131, 40815. doi:[10.1002/app.40815](https://doi.org/10.1002/app.40815).
- Sajid, M., 2016. Toxicity of nanoscale metal organic frameworks: A perspective. *Environ. Sci. Pollut. Res.* 23, 14805–14807. doi:[10.1007/s11356-016-7053-y](https://doi.org/10.1007/s11356-016-7053-y).
- Schllichte, K., Kratzke, T., Kaskel, S., 2004. Improved synthesis, thermal stability and catalytic properties of the metal-organic framework compound Cu₃(BTC)₂. *Micropor. Mesopor. Mater.* 73, 81–88. doi:[10.1016/j.micromeso.2003.12.027](https://doi.org/10.1016/j.micromeso.2003.12.027).
- Sharma, V.K., Feng, M., 2017. Water depollution using metal-organic frameworks-catalyzed advanced oxidation processes: A review. *J. Hazard. Mater.* 372, 3–16. doi:[10.1016/j.jhazmat.2017.09.043](https://doi.org/10.1016/j.jhazmat.2017.09.043).
- Shu, J.C., Yang, X.Y., Zhang, X.R., Huang, X.Y., Cao, M.S., Li, L., Yang, H.J., Cao, W.Q., 2020. Tailoring MOF-based materials to tune electromagnetic property for great microwave absorbers and devices. *Carbon.* 162, 157–171. doi:[10.1016/j.carbon.2020.02.047](https://doi.org/10.1016/j.carbon.2020.02.047).
- Simon-Yarza, T., Baati, T., Neffati, F., Njim, L., Couvreur, P., Serre, C., Gref, R., Najjar, M.F., Zakhama, A., Horcajada, P., 2016. In vivo behavior of MIL-100 nanoparticles at early times after intravenous administration. *Int. J. Pharmaceut.* 511, 1042–1047. doi:[10.1016/j.ijpharm.2016.08.010](https://doi.org/10.1016/j.ijpharm.2016.08.010).
- Solanky, D., Haydel, S.E., 2012. Adaptation of the neutral bacterial comet assay to assess antimicrobial-mediated DNA double-strand breaks in *Escherichia coli*. *J. Microbiol. Meth.* 91, 257–261. doi:[10.1016/j.mimet.2012.08.009](https://doi.org/10.1016/j.mimet.2012.08.009).
- Solioz, M., Abicht, H.K., Mermoud, M., Mancini, S., 2010. Response of gram-positive bacteria to copper stress. *J. Biol. Inorg. Chem.* 15, 3–14. doi:[10.1007/s00775-009-0588-3](https://doi.org/10.1007/s00775-009-0588-3).
- Sun, Z.G., Li, G., Zhang, Y., Liu, H., Gao, X., 2015. Ag-Cu-BTC prepared by postsynthetic exchange as effective catalyst for selective oxidation of toluene to benzaldehyde. *Catal. Commun.* 59, 92–96. doi:[10.1016/j.catcom.2014.09.047](https://doi.org/10.1016/j.catcom.2014.09.047).
- Tadjarodi, A., Abbaszadeh, A., 2016. A magnetic nanocomposite prepared from chelator-modified magnetite (Fe₃O₄) and HKUST-1 (MOF-199) for separation and preconcentration of mercury (II). *Microchim. Acta* 183, 1391–1399. doi:[10.1007/s00604-016-1770-2](https://doi.org/10.1007/s00604-016-1770-2).
- Tamames-Tabar, C., Cunha, D., Imbuluzqueta, E., Ragon, F., Serre, C., Blancoprieto, M.J., Horcajada, P., 2014. Cytotoxicity of nanoscaled metal-organic frameworks. *J. Mater. Chem. B*, 2, 262–271. doi:[10.1039/C3TB20832J](https://doi.org/10.1039/C3TB20832J).
- Wagner, A., Liu, Q., Rose, O.L., Eden, A., Vijay, A., Rojanasakul, Y., Dinu, C.Z., 2019. Toxicity screening of two prevalent metal organic frameworks for therapeutic use in human lung epithelial cells. *Int. J. Nanomed.* 14, 7583–7591. doi:[10.2147/JIN.S215950](https://doi.org/10.2147/JIN.S215950).
- Wang, C., Qian, X.R., An, X.H., 2015. In situ green preparation and antibacterial activity of copper-based metal-organic frameworks/cellulose fibers (HKUST-1/CF) composite. *Cellulose* 22, 3789–3797. doi:[10.1007/s10570-015-0754-4](https://doi.org/10.1007/s10570-015-0754-4).
- Wang, L.W., Hou, D.Y., Cao, Y.N., Ok, Y.S., Tack, F.M.G., Rinklebe, J., O'Connor, D., 2020. Remediation of mercury contaminated soil, water, and air: A review of emerging materials and innovative technologies. *Environ. Int.* 134, 105281. doi:[10.1016/j.envint.2019.105281](https://doi.org/10.1016/j.envint.2019.105281).
- Wu, D., Su, Q.Q., Li, Y., Zhang, C., Qin, X., Liu, Y.Y., Xi, W.S., Gao, Y.F., Cao, A.N., Liu, X.G., Wang, H.F., 2018. Toxic assessment and mechanistic investigation of engineered monoclinic VO₂ nanoparticles. *Nanoscale* 10, 9736–9746. doi:[10.1039/C8NR02224K](https://doi.org/10.1039/C8NR02224K).
- Wu, W.F., Li, Z.J., Chen, Y., Li, W.B., 2019. Polydopamine-modified metal-organic framework membrane with enhanced selectivity for carbon capture. *Environ. Sci. Technol.* 53, 3764–3772. doi:[10.1021/acs.est.9b00408](https://doi.org/10.1021/acs.est.9b00408).
- Xiao, J.D., Jiang, H.L., 2019. Metal-organic frameworks for photocatalysis and photothermal catalysis. *Acc. Chem. Res.* 52, 356–366. doi:[10.1021/acs.accounts.8b00521](https://doi.org/10.1021/acs.accounts.8b00521).
- Yen, C.I., Liu, S.M., Lo, W.S., Wu, J.W., Liu, Y.H., Chein, R.J., Yang, R.Q., Wu, K.C.W., Hwu, J.R., Ma, N.H., 2016. Cytotoxicity of postmodified zeolitic imidazolate framework-90 (ZIF-90) nanocrystals: Correlation between functionality and toxicity. *Chem. Eur. J.* 22, 2925–2929. doi:[10.1002/chem.201505005](https://doi.org/10.1002/chem.201505005).
- Zhang, Q.R., Xia, T., Zhang, C.D., 2020. Chronic exposure to titanium dioxide nanoparticles induces commensals-to-pathogen transition in *Escherichia coli*. *Environ. Sci. Technol.* 54, 13186–13196. doi:[10.1021/acs.est.0c04968](https://doi.org/10.1021/acs.est.0c04968).